Chinese Journal of Natural Medicines

Oroxylin A inhibits UVB-induced non-melanoma skin cancer by regulating XPA degradation

Renjie Dou, Jiarui Sun, Hang Yang, Yufen Zheng, Kang Yuan, Lei Qiang, Run Ma, Yunyao Liu

Citation: Renjie Dou, Jiarui Sun, Hang Yang, Yufen Zheng, Kang Yuan, Lei Qiang, Run Ma, Yunyao Liu, Oroxylin A inhibits UVB-induced non-melanoma skin cancer by regulating XPA degradation, Chinese Journal of Natural Medicines, 2025, 23(6), 742-753. doi: 10.1016/S1875-5364(25)60893-4.

View online: https://doi.org/10.1016/S1875-5364(25)60893-4

Chinese Journal of Natural Medicines 23 (2025) 742-753

Contents lists available at ScienceDirect

Chinese Journal of Natural Medicines

journal homepage: www.cjnmcpu.com/

Original article

Oroxylin A inhibits UVB-induced non-melanoma skin cancer by regulating XPA degradation

Renjie Dou[a,Δ], Jiarui Sun[a,Δ], Hang Yang[d,Δ], Yufen Zheng[e], Kang Yuan[f], Lei Qiang[a,*], Run Ma[c,*], Yunyao Liu[b,*]

[a] *State Key Laboratory of Natural Medicines, School of Basic Medicine and Clinical Pharmacy, China Pharmaceutical University, Nanjing 211198, China*
[b] *Jiangsu Key Laboratory of Molecular Biology for Skin Diseases and STIs, Institute of Dermatology, Chinese Academy of Medical Sciences & Peking Union Medical College, Nanjing 210042, China*
[c] *Clinical Laboratory Department, The Second Affiliated Hospital of Kunming Medical University, Kunming 650101, China*
[d] *The Third Department of Pharmacy, The First Affiliated Hospital of Henan Polytechnic University, Henan 454001, China*
[e] *Department of Basic Medicine and Clinical Pharmacy, School of Basic Medicine and Clinical Pharmacy, China Pharmaceutical University, Nanjing 211198, China*
[f] *School of Life Science and Technology, China Pharmaceutical University, Nanjing 211198, China*

ARTICLE INFO

Article history:
Received 7 April 2024
Revised 26 June 2024
Accepted 12 July 2024
Available online 20 July 2025

Keywords:
Non-melanoma skin cancer
Oroxylin A
XPA
GRP94
MDM2

ABSTRACT

Oroxylin A (OA), a natural compound extracted from *Scutellaria baicalensis*, demonstrates preventive potential against ultraviolet B (UVB)-induced non-melanoma skin cancer (NMSC), the most prevalent cancer worldwide with increasing incidence. Utilizing SKH-1 hairless mice exposed to UVB, this study showed that OA delayed NMSC onset and alleviated acute skin damage. Mechanistic investigations revealed its dual action: inhibiting inflammation and enhancing nucleotide excision repair (NER) by stabilizing XPA, a crucial deoxyribonucleic acid (DNA) repair protein. This stabilization occurred through OA's interaction with glucose-regulated protein 94 (GRP94), which disrupted murine double minute 2 (MDM2)-mediated XPA ubiquitination and proteasomal degradation. By maintaining XPA levels, OA expedited photoproduct clearance and diminished genomic instability, ultimately impeding NMSC development. These findings suggest OA as a promising chemopreventive agent targeting the GRP94/MDM2-XPA axis to counteract UVB-induced carcinogenesis.

1. Introduction

Skin cancer represents one of the most prevalent cancers among Caucasians, constituting 4% to 5% of all diagnosed cancers. It can be broadly categorized into two types: non-melanoma skin cancer (NMSC) and melanoma [1]. NMSCs primarily consist of basal cell carcinoma (BCC) and squamous cell carcinoma (SCC) [2]. BCC generally exhibits a low degree of malignancy, with limited capacity for local invasion, tissue destruction, and recurrence. In contrast, SCC demonstrates a higher propensity for metastasis, with metastasis rates ranging from 0.1% to 9.9%, and accounts for 75% of NMSC-related deaths [3]. While several known risk factors contribute to NMSC development, the cumulative effect of ultraviolet radiation (UVR) remains the most significant etiological factor [4]. UVR not only directly induces deoxyribonucleic acid (DNA) damage but also triggers an inflammatory state in the skin, with chronic low-grade inflammation stimulating counteracting immunosuppression [5-7]. Among all UV wavelengths, ultraviolet B (UVB) presents the highest risk. It can be absorbed by DNA, directly causing DNA damage and evoking skin inflammation, thereby leading to NMSC formation [8].

Among various types of DNA damage, UVB directly induces the formation of cyclobutane pyrimidine dimer (CPD) and 6-4-photoproduct (6-4PP). Nucleotide excision repair (NER) is one of the most fundamental and versatile DNA repair mechanisms, capable of accurately identifying and repairing CPD and 6-4PP [9]. Due to NER's inability to repair UV-induced lesions, xeroderma pigmentosum patients exhibit an elevated risk for UV-induced NMSC [10]. XPA, the primary subunit of the NER system, comprises three distinct domains: a central globular domain and dynamically disordered *N*- and *C*-terminal domains, which effectively recognize DNA damage and subsequently recruit NER proteins to the affected area [11, 12]. The observation that XPA patients display the most severe phenotype among XP patients underscores the crucial cellular role of XPA, prompting the current development of several XPA inhibitors [13-17].

Oroxylin A (OA), a bioactive flavonoid extracted from *Scutellaria baicalensis* Georgi, has demonstrated notable anti-cancer properties in previous studies. These properties include inhibiting cancer cell proliferation, suppressing cancer cell metabolism, inducing cancer cell apoptosis, inhibiting cancer cell invasion and metastasis, and reversing cancer cell resistance to chemotherapeutic agents [18-21]. In the present study, we examined the efficacy of OA in inhibiting UVB-induced inflammation and NMSC. Our

* Corresponding author.
E-mail addresses: yunyaoliu@cpu.edu.cn (Y. Liu); lqiang@cpu.edu.cn (L. Qiang); 467161115@qq.com (R. Ma)
Δ These authors contributed equally to this work.

https://doi.org/10.1016/S1875-5364(25)60893-4

findings reveal that OA binds to glucose-regulated protein 94 (GRP94), as demonstrated through pull-down assay, and inhibits murine double minute 2 (MDM2)-mediated ubiquitin-proteasomal degradation of XPA, thereby promoting the NER process.

2. Materials and methods

2.1. Animals and UVB irradiation

SKH-1 hairless mice were utilized for UVB irradiation experiments. The mice were subjected to sham, chronic UVB, or acute UVB irradiation as described in a previous study [22]. OA (purity > 99%) and Biotin-OA (purity > 99%) were generously provided by Prof. Zhiyu Li (China Pharmaceutical University, Nanjing, China). For topical application, OA was diluted to 100 μmol·L^{-1} with dimethyl sulfoxide (DMSO) (Sigma Aldrich, St. Louis, USA, D2650) and acetone (Nanjing Chemical Reagent, Nanjing, China, 67-64-1), with a DMSO to acetone volume ratio of 1∶1. The sham and vehicle group mice received 0.2 mL solvent on their backs, while the drug group mice received 0.2 mL OA solution 30 min prior to irradiation [23, 24]. For oral administration, OA and arginine (MD Bio. Inc, Z9001701, OA/arginine = 1∶4, *W/W*) were dissolved in saline with 10% PEG400 (*V/V*) (MedChemExpress, Monmouth Junction, NJ, USA, HY-Y0873A) and administered daily *via* intragastric route to each mouse. For chronic UVB irradiation and tumorigenesis studies, 24 mice were randomly allocated into three groups. The UVB + vehicle group and UVB + OA group mice were exposed to UVB irradiation every other day for 27 weeks, and tumor formation was documented. The initial UVB dosage was 80 mJ·cm^{-2} for the first week, followed by a weekly 10% increase until reaching 100 mJ·cm^{-2}. For acute UVB treatment, 18 mice were randomly divided into three groups. The UVB + vehicle group and UVB + OA group mice received UVB irradiation (100 mJ·cm^{-2}) 3 times every other day, with skin samples collected 24 h after the final UVB exposure. All animals were maintained under standard specific-pathogen-free conditions. The animal studies were conducted in accordance with protocols approved by the Animal Welfare and Ethics Committee of China Pharmaceutical University (2021-03-026).

2.2. Cell culture

Human immortal keratinocyte line (HaCaT) cells were obtained from the Cell Bank of Shanghai Institute of Biochemistry & Cell Biology, Chinese Academy of Sciences (China). HEK 293T cells were procured from the American Type Culture Collection (USA). Both cell lines were cultured in Dulbecco's modified Eagle medium (DMEM) (Invitrogen, Carlsbad, CA, 11965092), supplemented with 10% fetal bovine serum (Gibco, Grand Island, USA, A5256701) and 1% penicillin/streptomycin (Gibco, Grand Island, USA, 15140122). The cells were maintained at 37 °C in a humidified incubator (Bio-Rad, Hercules, CA, USA, PowerPac HC High-Current Power Supply) with 5% CO_2.

2.3. Histological and immunohistochemical staining

Dorsal skin samples, fixed with paraformaldehyde, were embedded in paraffin and stained using standard methods. Haematoxylin-eosin (H&E) staining was employed to examine skin morphology and tumor size. Immunohistochemistry was used to quantify the levels of Ki67 (Abcam, Cambridge, MA, AB-15580, 1∶1000) and γ-H2AX (Santa Cruz Biotechnology, CA, USA, sc-517348, 1∶200) in skin tissue. Images of these stained sections were captured randomly using an Olympus IX71 microscope (Japan).

2.4. Immunofluorescence staining

Immunofluorescence was employed to evaluate protein expression in skin tissue. Dorsal skins were fixed with 4% paraformaldehyde for 15 min. Following a wash in 10% phosphate-buffered saline (PBS), the slides were permeabilized with 0.2% Triton X-100 (Sigma Aldrich, St. Louis, USA, 9036-19-5) in PBS and subsequently blocked with 4% bovine serum albumin (Solarbio, Shanghai, China, A8020) for 1 h at room temperature. After incubation with MPO (Santa Cruz Biotechnology, CA, USA, sc-52707, 1∶200) and F4/80 (Santa Cruz Biotechnology, CA, USA, sc-52664, 1∶200) overnight at 4 °C, the slides were washed with PBS and then incubated with Alexa Fluor 647s antibody (Bioss, Woburn, USA, bs-0295G-AF647, 1∶200). The cells were stained with nuclear dye DAPI (Solarbio, Shanghai, China, C0080, 1 μg·mL^{-1}). All images were captured using a fluorescence microscope, and representative images were presented.

2.5. Quantitative real time-PCR

Total ribonucleic acid (RNA) was extracted from HaCaT and 293T cells using an RNA extraction kit (Vazyme Biotech, Nanjing, China, R401-01) following the manufacturer's instructions. The extracted RNA was then reverse transcribed into cDNA using HiScript II Q RT SuperMix for qPCR (Vazyme Biotech, Nanjing, China, R223-01). qPCR was performed using the Light Cycler 480 II real-time PCR system (Roche, Germany) with ChamQ SYBR qPCR Master Mix (Vazyme Biotech, Nanjing, China, Q331-02). The specific primers utilized in this study are detailed in Supplementary Table S1.

2.6. Plasmids construction

The XPA promoters were cloned from genomic DNA extracted from NHEK cells, utilizing publicly accessible sequence data. A nested PCR approach was employed to successfully clone the promoters. Subsequently, the PCR product underwent digestion and was cloned into pGL3-basic vectors. DNA fragments encoding GRP94-short hairpin RNA (shRNA) and XPA-shRNA were inserted into the pLKO.1 vector. The primers used in these procedures are detailed in Supplementary Table S2. All constructed plasmids were verified through sequencing to ensure accuracy.

2.7. Lentiviral infection

HEK 293T cells were cultured in fresh DMEM for 24 h prior to transfection. The cells were then co-transfected with destination plasmids and packaging plasmids (psPAX2 and pMD2G) using Lipofectamine™ 2000 transfection reagent (Invitrogen, Carlsbad, CA, 11668019). Culture media containing viral particles was collected at 48 and 72 h post-transfection. HaCaT cells were subsequently incubated with a 1∶1 mixture of virus-containing media and culture media for 24 h, supplemented with 8 μg·mL^{-1} polybrene (Sigma Aldrich, St. Louis, USA, TR-1003-G). This was followed by a 10-day antibiotic selection period.

2.8. Western blot

Cells were lysed using cell lysates containing RIPA buffer (Thermo Fisher Scientific, Waltham, MA, USA, 89901) and protease cocktail (Thermo Fisher Scientific, Waltham, MA, USA, 78429) for 30 min. After subjecting the protein lysate to polyacrylamide gel electrophoresis, the nitrocellulose membrane (Millipore, USA, HATF00010) was probed with specific antibodies. Images were captured using the Bio-Rad system to identify the antibody binding position and intensity. The following primary antibodies were utilized: GAPDH (Santa Cruz Biotechnology, CA, USA,

sc-32233, 1∶5000), γ-H2AX (Santa Cruz Biotechnology, CA, USA, sc-517348, 1∶1000), GRP94 (Proteintech, Manchester, UK, 14700-1-AP, 1∶1000) and XPA (HUABIO, Zhejiang, China, HA500133, 1∶1000).

2.9. Immunoprecipitation (IP)

Cells underwent lysis in IP buffer [50 mmol·L^{-1} tris-HCl, 150 mmol·L^{-1} NaCl, 1 mmol·L^{-1} EDTA, and 1% NP-40 (pH 7.4)] containing protease inhibitor cocktail. The cell lysate was subsequently sonicated, clarified, and incubated with antibodies against XPA (1∶100) overnight at 4 °C, followed by a 4-h incubation with Protein A/G Magnetic Beads (MedChemExpress, Monmouth Junction, NJ, USA, HY-K0202) at 4 °C. The resulting immunocomplexes were then subjected to immunoblot analysis.

2.10. Slot blot

Slot blot assays for CPD and 6-4PP were conducted according to previously established protocols [25]. In summary, cells were harvested at various time intervals following OA administration, and DNA was extracted using the FastPure Cell/Tissue DNA Isolation Mini Kit (Vazyme Biotech, Nanjing, China). DNA concentration was determined by measuring absorbance at 260 nm using a NanoDrop 1000 spectrophotometer (NanoDrop products, Wilmington, DE). Quantification of CPD and 6-4PP in DNA samples was performed *via* slot blot analysis (Bio-Rad) utilizing CPD (COSMO BIO Co., Koto-Ku, Tokyo, Japan, TDM-2) and 6-4PP (COSMO BIO Co., Koto-Ku, Tokyo, Japan, TM-P-07) monoantibodies.

2.11. Dual-luciferase reporter assay

The luciferase assay involved transfecting pGL3 XPA long-Luc, pGL3 XPA short-Luc plasmids, and pRL-TK (serving as a transfection efficiency control) using Lipofectamine™ 2000 transfection reagent. Luciferase activity was subsequently detected using a dual luciferase reporter assay kit (Vazyme Biotech, Nanjing, China), following the manufacturer's protocol. The luciferase activity was quantified as the ratio of the firefly luciferase signal to the renilla luciferase signal.

2.12. Silver staining

Cells were lysed to obtain protein samples, which were then incubated with Biotin or Biotin-OA at 4 °C overnight to yield a peptide mixture. The polypeptide mixtures were subsequently separated by sodium dodecyl sulfate-polyacrylamide gel electrophoresis (SDS-PAGE), and the polypeptide bands were visualized using silver staining. The differentially stained silver band was then isolated for subsequent mass spectrometry analysis.

2.13. Mass spectrometry

Protein samples were separated using SDS-PAGE gels, and gel pieces were excised and destained with 30% acetonitrile/100 mmol·L^{-1} NH_4HCO_3 until clarification. The gels were subsequently dried in a vacuum centrifuge. In-gel proteins underwent reduction with dithiothreitol (10 mmol·L^{-1} dithiothreitol/100 mmol·L^{-1} NH_4HCO_3) for 30 min at 56 °C, followed by alkylation with iodoacetamide (200 mmol·L^{-1} iodoacetamide/100 mmol·L^{-1} NH_4HCO_3) in darkness at room temperature for 30 min. The gel pieces were briefly rinsed with 100 mmol·L^{-1} NH_4HCO_3 and acetonitrile, then digested overnight in 12.5 ng·μL^{-1} trypsin (Promega, Madison, WI, USA, V5111) in 25 mmol·L^{-1} NH_4HCO_3. Peptide extraction was performed thrice using 60% acetonitrile/0.1% trifluoroacetic acid. The extracts were pooled and completely dried *via* vacuum centrifugation. Sample analysis was conducted on an EASY-nLC 1000 UHPLC system coupled to a Q Exactive HF-X mass spectrometer (Thermo Fisher Scientific). The mass spectrometer operated in positive ion mode. Mass spectrometry data acquisition employed a data-dependent top 10 method, dynamically selecting the most abundant precursor ions from the survey scan (*m/z* 300–1800) for higher-energy collisional dissociation fragmentation. The automatic gain control target was set to 3×10^6, with a maximum inject time of 10 ms. Dynamic exclusion duration was 40.0 s. Survey scans were acquired at a resolution of *m/z* 70 000 at 200, while a resolution for higher-energy collisional dissociation spectra was set to *m/z* 17 500 at 200, with an isolation width of *m/z* 2. The normalized collision energy was 30 eV, and the underfill ratio, specifying the minimum percentage of the target value likely to be reached at maximum fill time, was defined as 0.1%. The instrument operated with peptide recognition mode enabled. Raw files were searched against the corresponding database using Mascot2.2 software.

2.14. Microscale thermophoresis (MST)

The binding studies between OA and GRP94 were conducted using a Monolith NT.115 instrument (Nanotemper Technologies, Munich, Germany), following the manufacturer's prescribed protocols.

2.15. Molecular docking

The crystal structures of GRP94 (Protein Data Bank [PDB] ID: 5ULS) were obtained from the PDB and prepared using the Protein Preparation Wizard in the Schrodinger suite. Small molecules were processed using the LigPrep module of Schrodinger. The Glide module (extra precision [XP] mode) was employed for molecular docking, chosen for its superior performance in self-docking analysis. The top ten poses of each ligand underwent minimization through a post-docking program, with the optimal pose retained for subsequent analysis.

2.16. Statistical analysis

All data were presented as mean ± standard error of the mean (SEM). Statistical analysis was conducted using unpaired *t*-tests, one-way analysis of variance (ANOVA), and two-way ANOVA with Tukey's test. Statistical significance was defined as $P < 0.05$.

3. Results

3.1. OA inhibits UVB-induced NMSC

Previous studies have demonstrated that UVB exposure induces non-melanoma skin cancer in SKH-1 hairless mice [22]. The process of UVB-induced skin carcinogenesis and the subsequent intervention with oroxylin A in SKH-1 hairless mice are illustrated in Fig. 1A. As shown in Fig. 1B, compared to the sham group, UVB irradiation resulted in dry skin, the appearance of numerous papillary tumors on the dorsal side of the mice, and ulcer formation in some of the tumors. Tumor formation in UVB-exposed mice began around 15 weeks, whereas in oroxylin A-treated mice, tumors did not appear until 21 weeks, and the number of tumors was only half that of the UVB-only group (Figs. 1C and 1D). Histological analysis revealed that the sham group mice exhibited clear skin layers and complete structures, whereas UVB irradiation promoted excessive keratinocyte proliferation. Mice treated with OA maintained intact epidermal structure, clear layers, mild epidermal hyperplasia, minimal keratinization, and no apparent atypical cells (Figs. 1E and 1F). Immunohistochemical staining of Ki67 confirmed that UVB induced excessive keratino-

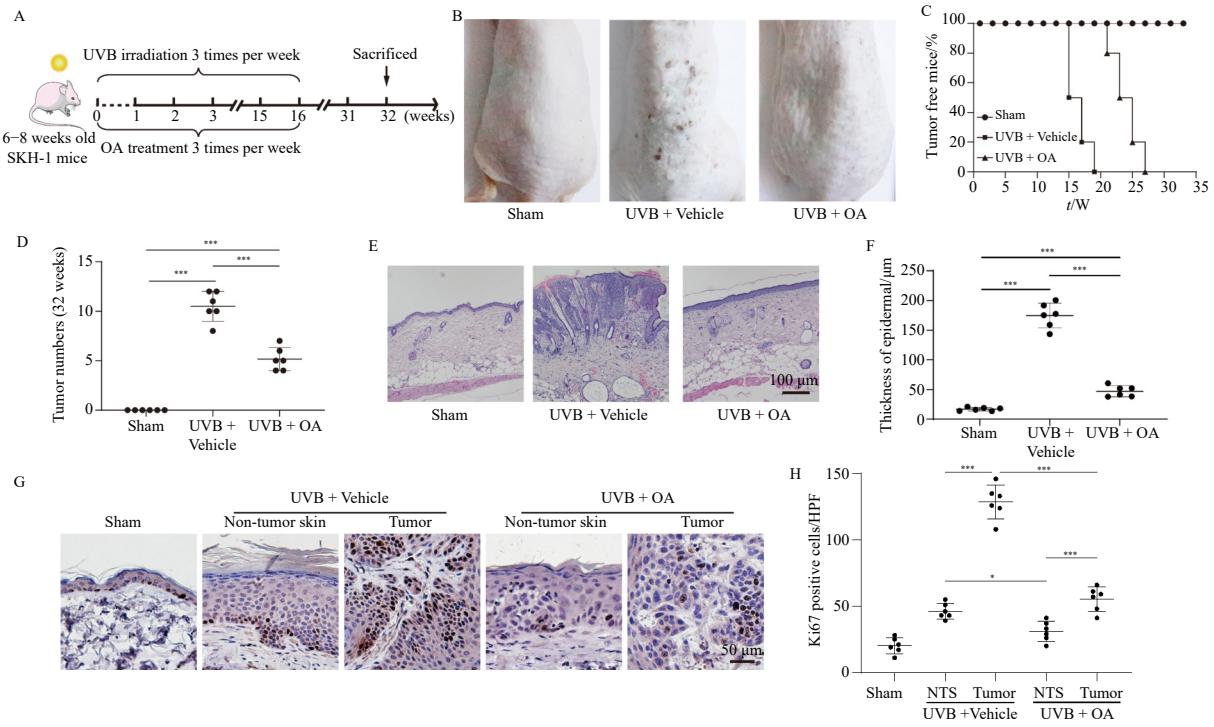

Fig. 1 Oroxylin A inhibits UVB-induced non-melanoma skin cancer. The vehicle group and the oroxylin A group SKH-1 mice were irradiated with UVB three times a week. The first irradiation dosage was 50 mJ·cm^{-2}, and each subsequent dosage was increased by 10% until the dosage was 100 mJ·cm^{-2}. UVB irradiation was discontinued until 16 weeks, and routine feeding was continued until 32 weeks. All mice were sacrificed and dorsal skin samples were taken. (A) A schematic for chronic UVB irradiation. (B) Representative photographs showing skin tumors induced by chronic UVB irradiation. (C) Percentage of tumor-free mice after chronic UVB irradiation. (D) Tumor numbers per mouse after chronic UVB irradiation. (E) Representative photomicrographs of HE staining of skin sections. (F) Quantification of epidermal thickness in sham, vehicle group, and oroxylin A group mice samples. (G) Representative immunohistochemical analysis of Ki67 in normal skin and tumor tissue. (H) Quantification of the Ki67 staining positive cell number as shown in G. Data are presented as mean ± SEM (n = 6), $^{*}P < 0.05$, $^{**}P < 0.01$, $^{***}P < 0.001$ *vs* Sham group or UVB + Vehical group. Differences are tested using two-way ANOVA.

cyte proliferation, while OA treatment mitigated this process (Figs. 1G and 1H). Additionally, we verified the efficacy of OA through intragastric administration. Results indicated that UVB irradiation led to sunburn, cutaneous vascular dilatation, epidermal thickening, and an increase in skin inflammatory cells. These conditions improved after intragastric administration of OA, particularly evident in Ki67-positive cells (Fig. S1). These findings suggest that OA can delay the onset of UVB-induced NMSC in SKH-1 hairless mice.

3.2. OA alleviates acute skin sunburn caused by UVB

UVB exposure has been established to promote epidermal hyperplasia and inflammatory cell infiltration [26, 27]. This study investigated the potential of OA in mitigating UVB-induced inflammatory conditions in the skin. As illustrated in Figs. 2A and 2B, UVB irradiation induced sunburn, characterized by an inflammatory response with cutaneous vasodilatation and increased vascular permeability. Administration of OA attenuated UVB-induced sunburn. Histological analysis revealed that, compared to UVB-irradiated mice, the OA treatment group exhibited resistance to UVB-induced epidermal hyperplasia and vascular leakage (Figs. 2C and 2D). Moreover, OA treatment reduced the number of Ki-67 positive cells (Figs. 2E and 2F). To determine an appropriate dosage of OA for the HaCaT cells in subsequent experiments, CCK-8 assay and TUNEL staining were employed, and 50 μmol·L^{-1} was selected (Figs. 3A and 3B). Concurrently, UVB irradiation was found to decrease the levels of inflammatory factors, including interleukin-1β (IL-1β), IL-6, IL-8, CXC chemokine ligand 1 (CXCL1), CXCL2, and CXCL9 (Fig. 3C). To assess the impact on the inflammatory microenvironment, an immunofluorescence assay was utilized to detect F4/80 and MPO expression, which are markers of macrophages and neutrophils respectively. As demonstrated in Figs. 3D and 3E, F4/80 and MPO expressions in the dermis were downregulated to varying degrees following OA administration. These findings indicate that OA inhibits UVB-induced vasodilatation, inflammation, and epidermal hyperplasia.

3.3. OA facilitates UVB-induced NER through upregulating XPA

UVB-induced DNA damage is a critical factor contributing to NMSC. This study investigated whether OA mitigated DNA damage. Results demonstrated that OA treatment reduced γ-H2AX levels in both mice skin and HaCaT cells, as evidenced by immunohistochemical staining (Figs. 4A and 4B) and Western blot analysis (Fig. 4C). A recent study indicated that OA could modulate NER-related proteins, which are crucial in repairing UVB-induced DNA damage [28]. Slot blot analysis was employed to examine the expression of DNA damage products 6-4PP and CPD. As illustrated in Figs. 4D–4G, OA administration significantly enhanced the repair of CPD and 6-4PP compared to the control group in HaCaT cells. Furthermore, as shown in Figs. 4H and 4I, immunofluorescence analysis of dorsal skin confirmed that OA could accelerate the removal of CPD and 6-4PP.

To investigate the mechanism by which OA regulates NER, we examined the expression of NER-related proteins. Western blot results indicated that XPA was significantly upregulated after OA treatment (Fig. 5A). OA also enhanced UVB-induced augmentation of XPA expression (Fig. 5B). As depicted in Fig. 5C, shXPA HaCaT cells were constructed. Suppression of XPA delayed OA-induced CPD and 6-4PP elimination, confirming that OA regulates NER function *via* XPA (Figs. 5D–5G). Several studies have reported that NER can regulate inflammation [29-31]. As shown in Fig. 5H, inflammation-associated cytokines and chemokines were detected, and results revealed that OA no longer downregulated UVB-induced inflammation in HaCaT shXPA cells. These findings suggest that OA might downregulate inflammation by regulating XPA in the initial stage of tumor development. Subsequently, we ex-

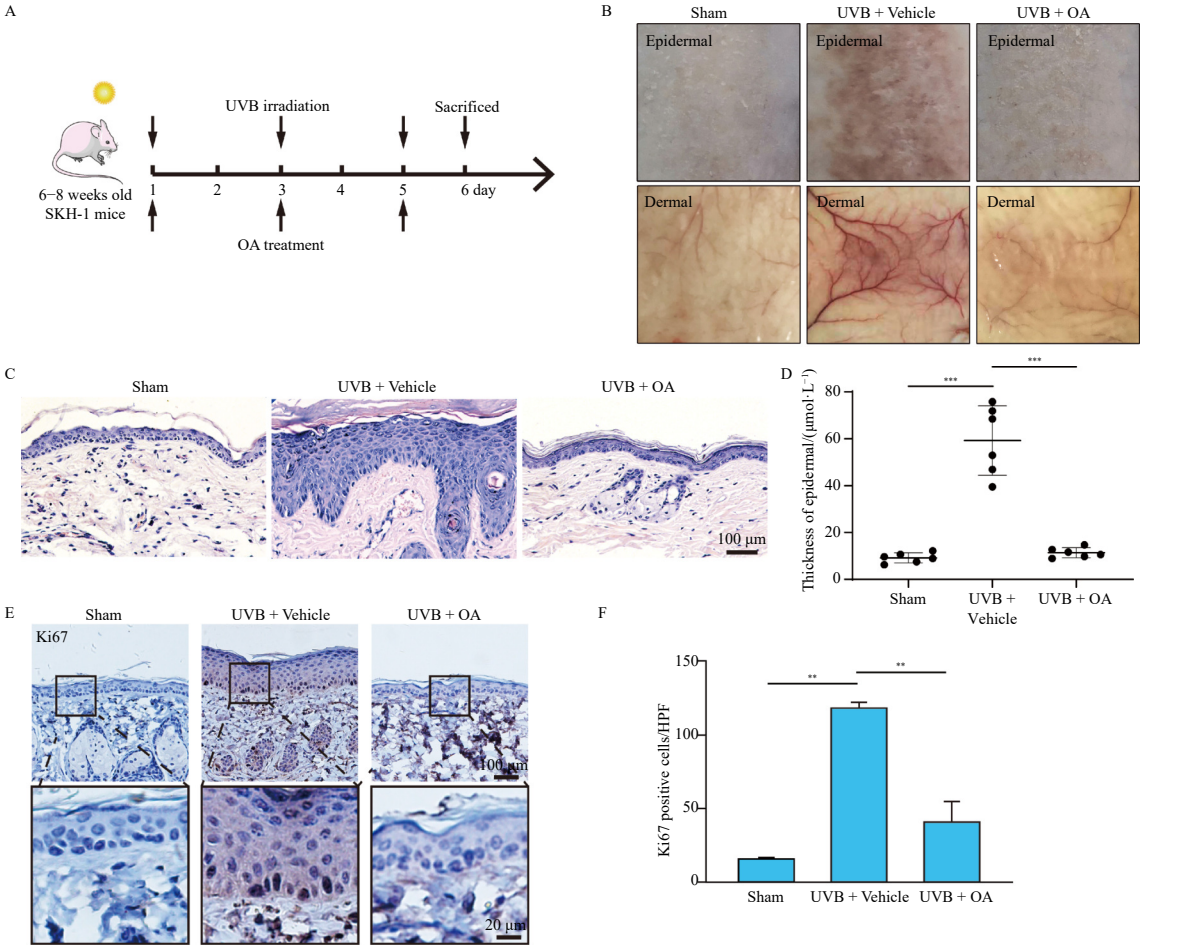

Fig. 2 Oroxylin A alleviates acute skin sunburn caused by UVB. The vehicle group and the oroxylin A group SKH-1 mice were exposed to acute UVB irradiation (3 times every other day). Skin samples were collected at 24 h post-final UVB for the indicated analysis. (A) A schematic for acute UVB irradiation. (B) Representative photographs showing sunburn induced by acute UVB irradiation. (C) Representative photomicrographs of HE staining of skin sections. (D) Quantification of epidermal thickness in sham, vehicle, and oroxylin A samples. (E) Representative immunohistochemical analysis of Ki67 in sham, vehicle, and oroxylin A group samples. (F) Quantification of the Ki67 staining positive cell number as shown in E. Data are presented as mean ± SEM (n = 6), $^{*}P < 0.05$, $^{**}P < 0.01$, $^{***}P < 0.001$ *vs* Sham group or UVB + Vehical group. Differences are tested using two-way ANOVA.

plored OA's role in the transcriptional activity of XPA using a luciferase reporter assay by constructing plasmids containing short or long XPA promoters (Fig. 5I). However, no significant differences were observed between these two groups in HaCaT or 293T cells (Figs. 5J and Figs. 5K). Next, we investigated the effect of OA on XPA messenger RNA (mRNA) stability. As shown in Fig. 5L, there were no differences between the control group and the OA group over time, indicating that OA does not regulate XPA by affecting the synthesis or degradation of its mRNA.

3.4. OA binds to GRP94

To elucidate the mechanism by which OA regulates XPA, cell protein lysates were incubated with Biotin and Biotin-OA, respectively, followed by electrophoresis and silver staining. The differential band was subsequently excised for mass spectrometry analysis. As illustrated in Fig. 6A, compared to the negative control band, the MS analysis identified a significantly enriched protein, GRP94. Subsequently, GRP94 recombinant protein was constructed, and MST analysis was performed to evaluate the dissociation kinetics of OA with GRP94. As shown in Fig. 6B, Biotin-OA exhibited binding affinity for GRP94, with a K_d value of approximately 12.04 μmol·L^{-1}, while the K_d value between GRP94 and OA was approximately 6.46 μmol·L^{-1}. Molecular docking simulations were then employed to investigate the binding between OA and the crystal structure of GRP94. The prediction results indicated that OA might form carbon-hydrogen bonds with GLY193 and PHE195 or hydrogen bonds with SER169, GLN194, VAL197, GLY198, and PHE199 (Fig. 6C). However, OA did not affect *GRP94* mRNA levels (Fig. 6D), and neither UVB irradiation nor OA altered the expression of GRP94 in HaCaT cells (Fig. 6E).

3.5. OA inhibits XPA degradation *via* the proteasome pathway

GRP94, the most abundant protein residing in the endoplasmic reticulum, is associated with oxidative stress, endoplasmic reticulum calcium depletion, and the accumulation of misfolded proteins [32]. To further investigate the role of GRP94 in OA-mediated upregulation of XPA, we established a stable GRP94 knockdown HaCaT cell line (Figs. 7A and 7B). Although OA does not affect the mRNA and protein levels of GRP94, inhibition of GRP94 resulted in attenuation of OA-induced XPA expression (Fig. 7B). Furthermore, as illustrated in Figs. 7C–7F, OA could no longer alter the percentage of CPD and 6-4PP repair in HaCaT shGRP94 cells. Collectively, these findings demonstrate that OA upregulates XPA through binding to GRP94.

A recent investigation indicated that OA may operate through proteasome-mediated degradation [33]. To elucidate whether OA could inhibit XPA degradation *via* the proteasome pathway, we treated HaCaT shCon and shGRP94 cells with the protein synthesis inhibitor CHX. In a CHX pulse-chase assay, we observed that the knockdown of GRP94 accelerated XPA degradation (Fig. 7G). Consequently, our findings demonstrate that OA enhances the stabil-

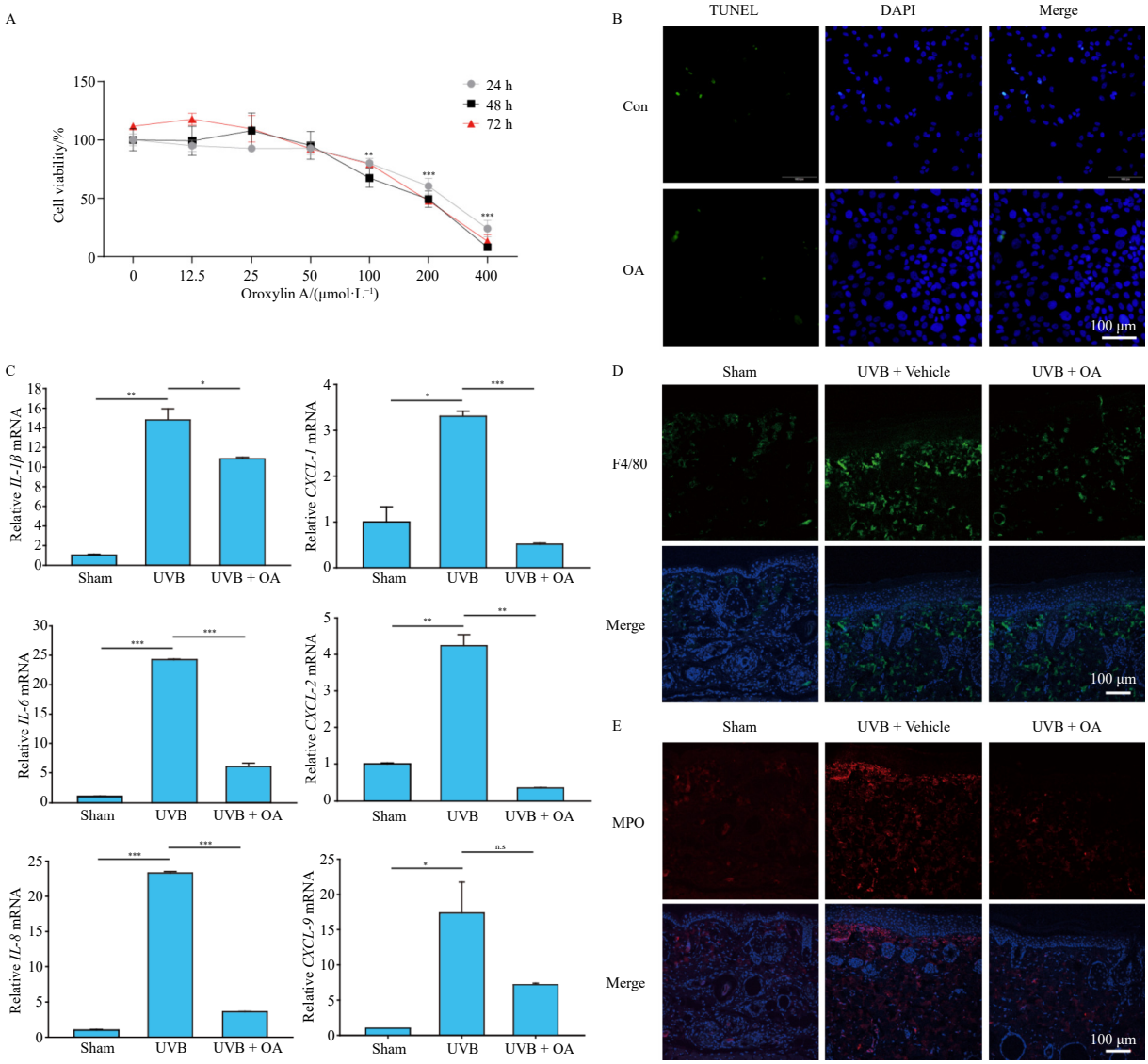

Fig. 3 Oroxylin A alleviates UVB-induced skin inflammation. (A) HaCaT cells were treated with varying doses of oroxylin A for different time points, and cell viability was analyzed by CCK-8 assay. (B) TUNEL staining was utilized to exclude the effect of oroxylin A on cell apoptosis. (C) HaCaT cells were treated with 50 μmol·L^{-1} oroxylin A and exposed to UVB irradiation (5 mJ·cm^{-2}) or left untreated. The mRNA levels of *IL-1β*, *IL-6*, *IL-8*, *CXCL-1*, *CXCL-2* and *CXCL-9* were measured through RT-qPCR, with GAPDH serving as an internal control. Immunofluorescence staining was used to detect the expressions of (D) F4/80 (red) and (E) MPO (red), with DAPI staining of nuclei (blue) for cellular localization. Results are presented as fold changes relative to control, with data expressed as the mean ± SEM (n = 3), $^{*}P < 0.05$, $^{**}P < 0.01$, $^{***}P < 0.001$ *vs* Sham group or UVB group (n.s., not significant). Differences are tested using two-way ANOVA.

ity of XPA protein through the proteasome pathway, and this process is dependent on GRP94.

MDM2, a critical negative regulator of p53, has been reported to interact with p53 and GRP94 to enhance MDM2-mediated p53 ubiquitination and degradation [34]. To investigate the role of MDM2 in XPA regulation, the MDM2 inhibitor SP141 was employed. SP141 inhibited XPA degradation in a dose-dependent manner, suggesting that MDM2 may regulate XPA degradation

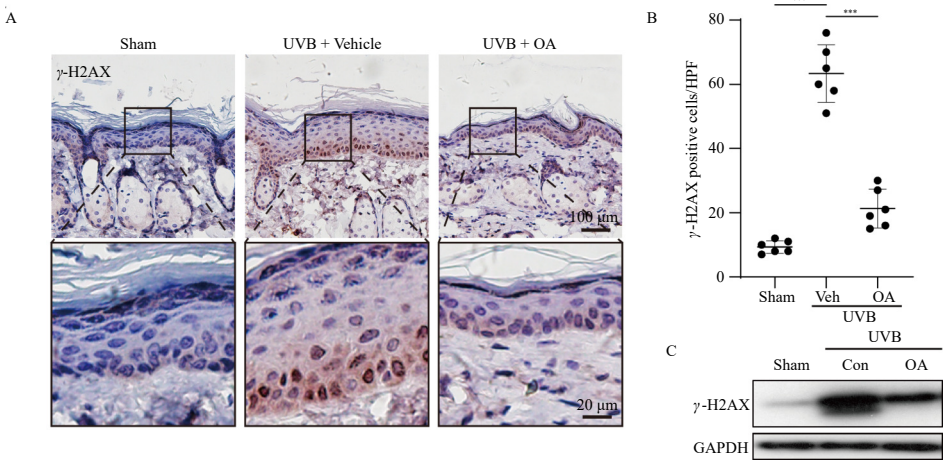

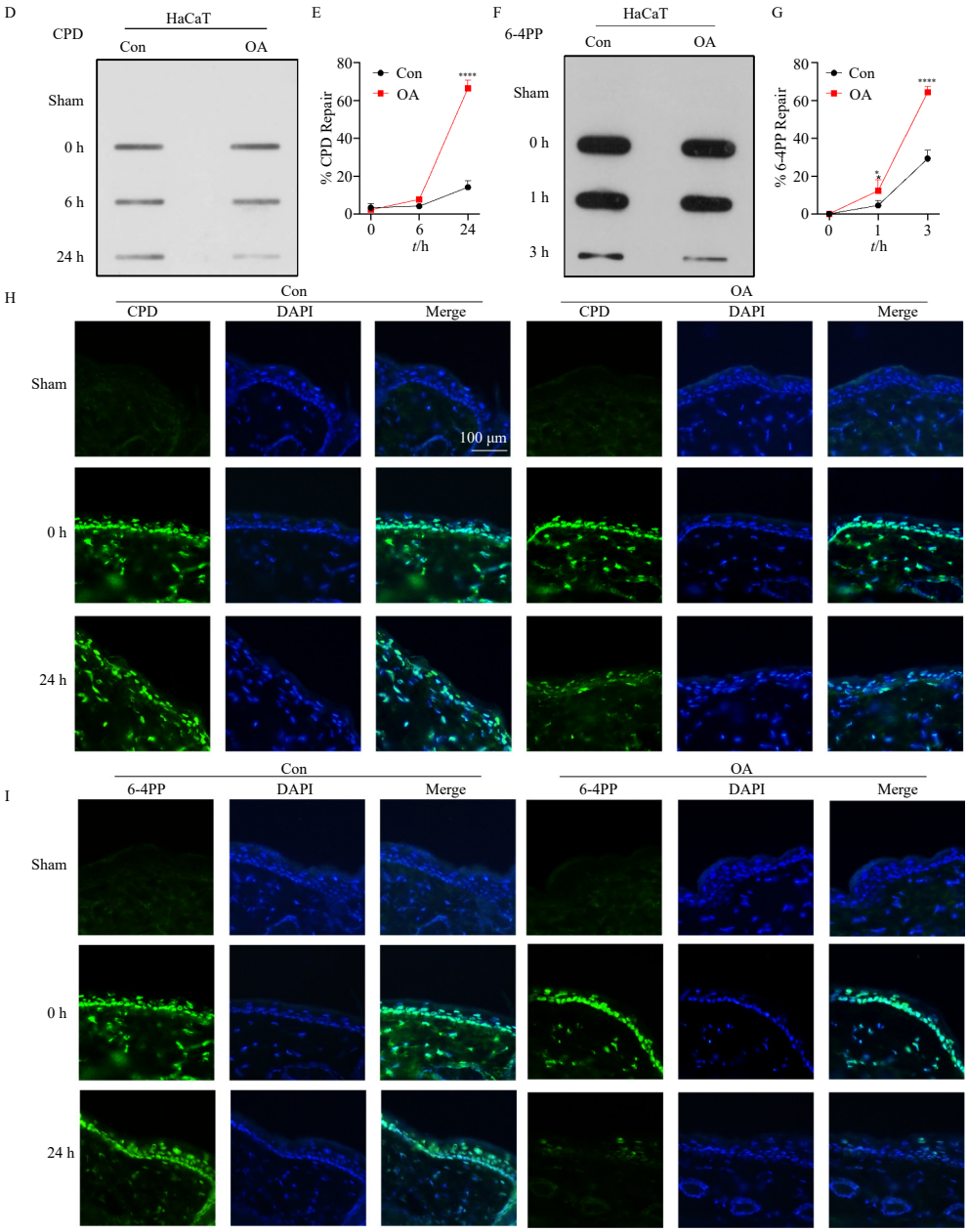

Fig. 4 Oroxylin A facilitates UVB-induced nucleotide excision repair. (A) Immunohistochemical staining of γ-H2AX. (B) Quantification of the γ-H2AX staining positive cell number as shown in Fig. 4A. (C) Western blot analysis of γ-H2AX and GAPDH in HaCaT cells treated with oroxylin A (50 μmol·L^{-1}) or DMSO for 24 h. Cells were collected for analysis at 24 h after UVB irradiation. (D) Slot blot analysis of CPD proteins in HaCaT cells treated with Oroxylin A (50 μmol·L^{-1}) or DMSO for 24 h. Cells were collected for analysis at 0, 6, and 24 h after UVB irradiation. (E) Quantification of the Slot blot analysis of CPD proteins. (F) Slot blot analysis of 6-4PP proteins in HaCaT cells treated with oroxylin A (50 μmol·L^{-1}) or DMSO for 24 h. Cells were collected for analysis at 0, 1, and 3 h after UVB irradiation. (G) Slot blot analysis of 6-4PP proteins. Representative images of (H) CPD and (I) 6-4PP immunofluorescence assay of mice dorsal skin in the presence or absence of 50 μmol·L^{-1} oroxylin A. Data are presented as mean ± SEM (n = 6), $^{*}P < 0.05$, $^{**}P < 0.01$, $^{***}P < 0.001$ (n.s. not significant). Differences are tested using two-way ANOVA.

(Fig. 7H). Both OA and SP141 significantly increased XPA expression individually, but no significant change in XPA expression was observed when OA and SP141 were administered simultaneously (Fig. 7I). Considering these findings, OA reduces MDM2-mediated XPA ubiquitination and degradation *via* binding GRP94, which affects NER and subsequently alters skin inflammation and the development of NMSC.

4. Discussion

UVB radiation is a primary contributor to NMSC [35]. Beyond directly causing DNA damage through skin penetration, UVB can induce skin oxidative stress, inflammation, and deleterious immune reactions, collectively promoting the initiation and progression of NMSC. The escalating incidence and risk of UVB-induced NMSC necessitate the development of novel therapeutic agents [36]. OA, extracted from the root bark of *Scutellaria baicalensis* Georgi, is a yellow needle-shaped crystal with the chemical formula $C_{16}H_{12}O_5$. Research has demonstrated that OA exhibits a broad spectrum of potent biological activities, including anti-tumor, anti-inflammatory, and neuroprotective effects, with its anti-tumor properties garnering significant research interest [18-20]. Studies indicate that pretreatment with OA significantly reduces tumor incidence and diversity in a DMBA/TPA-induced mouse skin tumor model. Furthermore, OA substantially inhibits TPA-induced inflammatory responses by suppressing the expression of the adapter protein SHCBP1 [37]. However, the potential of OA to inhibit UVB-induced NMSC remains unexplored. Our findings suggest that OA delays the onset of UVB-induced NMSC and mitigates UVB-induced acute skin damage.

The association between cancer and chronic inflammation has been recognized since the 19th century [38]. Inflammation serves as the body's immune defense mechanism against harmful stimuli. Persistent inflammatory stimulation and immune cell activation result in long-term repeated tissue destruction and regeneration, leading to chronic inflammation [39-41]. Several studies have reported that OA demonstrates anti-inflammatory properties [42, 43]. NER plays a crucial role in regulating inflammation by maintaining genomic stability, triggering the elimination of cells with irreparable DNA damage, and engaging in cell-extrinsic on-

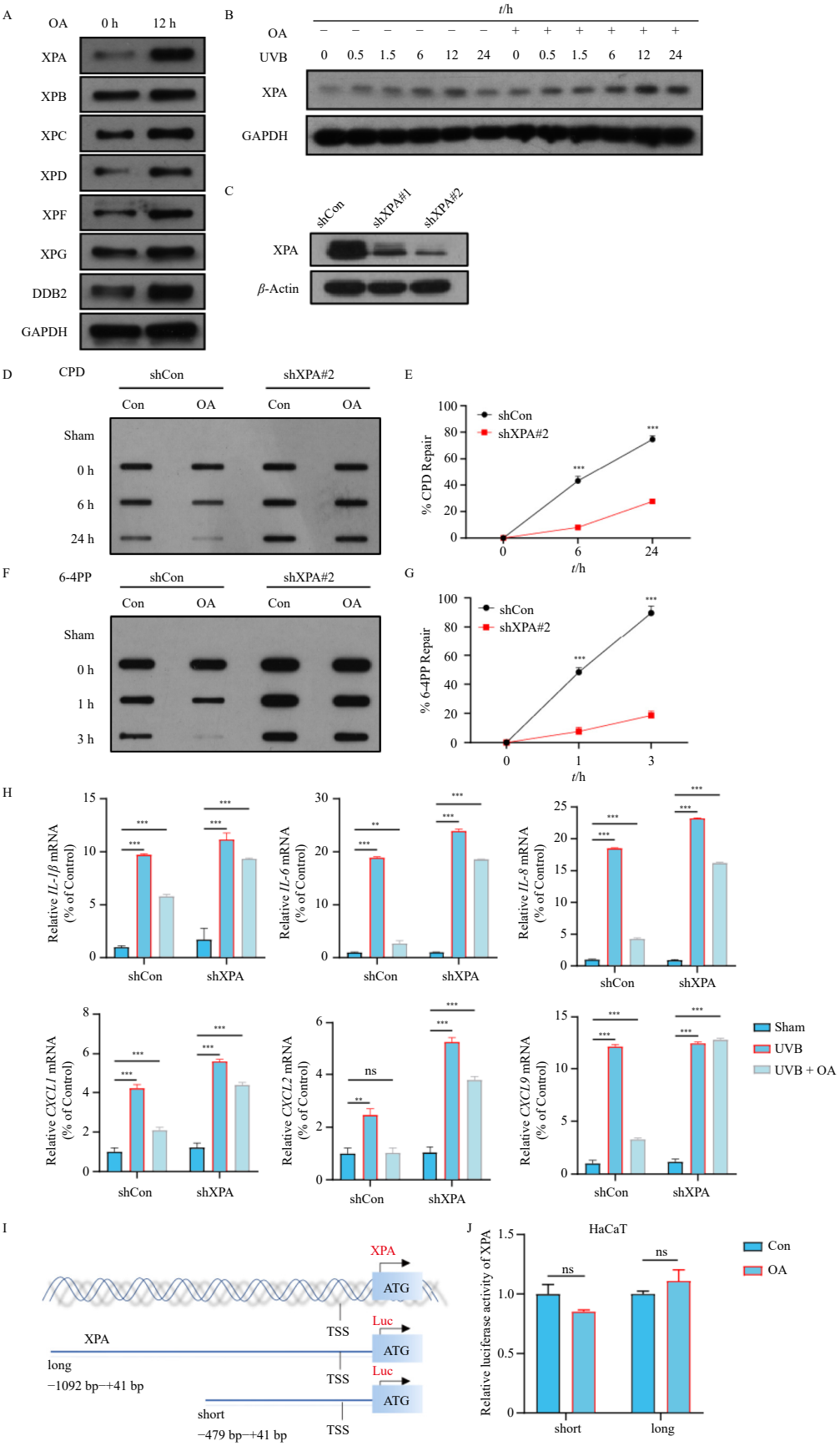

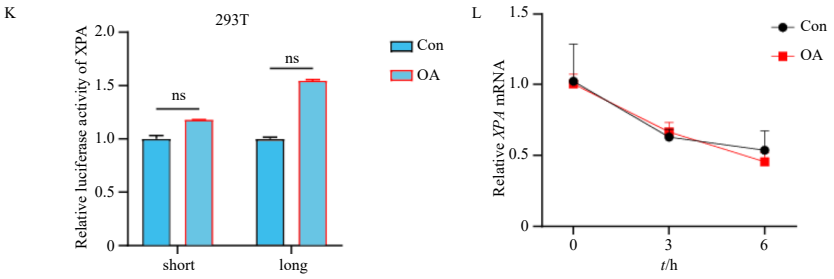

Fig. 5 Oroxylin A reinforces nucleotide excision repair through upregulating XPA. (A) HaCaT cells were treated with oroxylin A as indicated dosages for 12 h, and Western blot assay was used to evaluate the expression level of XPA, XPB, XPC, XPD, XPF, XPG, DDB2, GAPDH was used as a loading control. (B) Immunoblot analysis of XPA and GAPDH in HaCaT cells treated with or without oroxylin A at 0, 0.5, 1.5, 6, 12, and 24 h post-UVB (10 mJ·cm^{-2}). (C) The efficiency of XPA knockdown was verified by Western blot (XPA shRNA#1 and XPA shRNA#2). (D) Slot blot analysis of CPD proteins in HaCaT shCon and shXPA cells treated with Oroxylin A (50 μmol·L^{-1}) or DMSO for 24 h. Cells were collected for analysis at 0, 6, and 24 h after UVB irradiation. (E) Quantification of the Slot blot analysis of CPD proteins. (F) Slot blot analysis of 6-4PP proteins in HaCaT shCon and shXPA cells treated with oroxylin A (50 μmol·L^{-1}) or DMSO for 24 h. Cells were collected for analysis at 0, 1, and 3 h after UVB irradiation. (G) Slot blot analysis of 6-4PP proteins. (H) HaCaT shCon and shXPA cells were treated with 50 μmol·L^{-1} oroxylin A and irradiated with UVB (5 mJ·cm^{-2}) or not, mRNA levels of *IL-1β*, *IL-6*, *IL-8*, *CXCL-1*, *CXCL-2,* and *CXCL-9* were measured through RT-qPCR. *GAPDH* as an internal control. (I) A schematic for luciferase reporter gene construction. (J) HaCaT cells and (K) 293T cells were co-transfected with *XPA* short-Luc or *XPA* long-Luc with pRL-TK vectors (0.1 μg), respectively. After 24 h, cells were treated with 50 μmol·L^{-1} oroxylin A for 6 h, followed by luciferase reporter assay. (L) HaCaT cells were treated with oroxylin A and co-incubated with ACTD in a time-dependent manner, as indicated. The relative *XPA* mRNA level was measured by qPCR and *GAPDH* as an internal control. $^{*}P < 0.05$, $^{**}P < 0.01$, $^{***}P < 0.001$ (n.s. not significant). Differences are tested using two-way ANOVA.

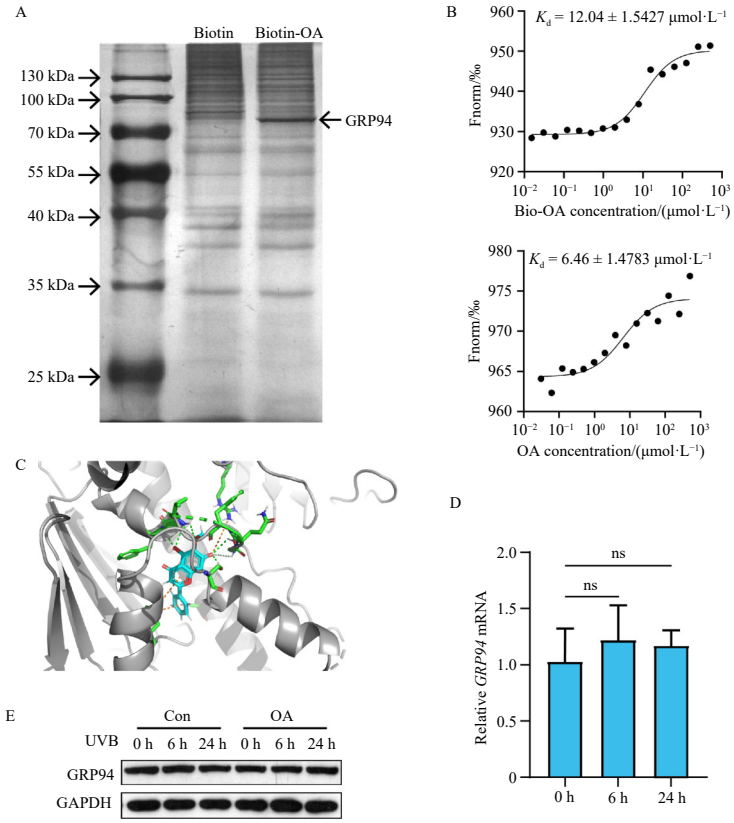

Fig. 6 Oroxylin A specifically binds GRP94. (A) Silver staining of Biotin and Biotin-OA. (B) Representative microscale thermophoresis (MST) analysis for the interaction of oroxylin A with human GST-GRP94 recombination protein. (C) Molecular docking analysis of the potential binding between oroxylin A and GRP94. (D) HaCaT cells were treated with oroxylin A (50 μmol·L^{-1}) for different time points, and *GRP94* mRNA levels were measured through RT-qPCR. Fold change is represented as the mean ± SEM (n = 3). (E) The level of GRP94 in HaCaT cells treated with oroxylin A or not after UVB irradiation for indicated hours.

cosuppression *via* immunosurveillance [44, 45], which aligns with our findings. Furthermore, our results indicate that OA exerts its anti-inflammatory effect through the regulation of NER, establishing a connection between UVB-induced acute inflammation and chronic UVB-induced NMSC.

The NER system plays a crucial role in protecting cells from damage induced by exogenous and intracellularly produced DNA-reactive molecules, particularly in regulating inflammation. The deficiency of XPA could enhance photobiologic reactions, including acute inflammation and immunosuppression [46, 47]. Previous research has shown that OA could down-regulate the transcription level of XPC in lung cancer cells under hypoxic conditions through HIF-1α but has no significant effect under normoxic conditions [28]. In the present study, OA promoted the stability of XPA by inhibiting ubiquitin proteasomal degradation in keratinocytes. In this process, MDM2 functions as a ubiquitin ligase. It has been reported that p53 is a GRP94 client protein, and GRP94 acts as a scaffolding protein to enhance MDM2 E3 ligase activity, thereby increasing p53 ubiquitination and degradation [33]. Our results suggest that MDM2 might be the ubiquitinase of XPA. However, the underlying mechanism requires further investigation and verification.

GRP94, also known as GP96, is encoded by the *hsp90b1* gene and is an intrinsic protein of the endoplasmic reticulum [48]. GRP94 functions as a molecular chaperone, facilitating protein folding, transport, secretion, and degradation. It is a member of the heat

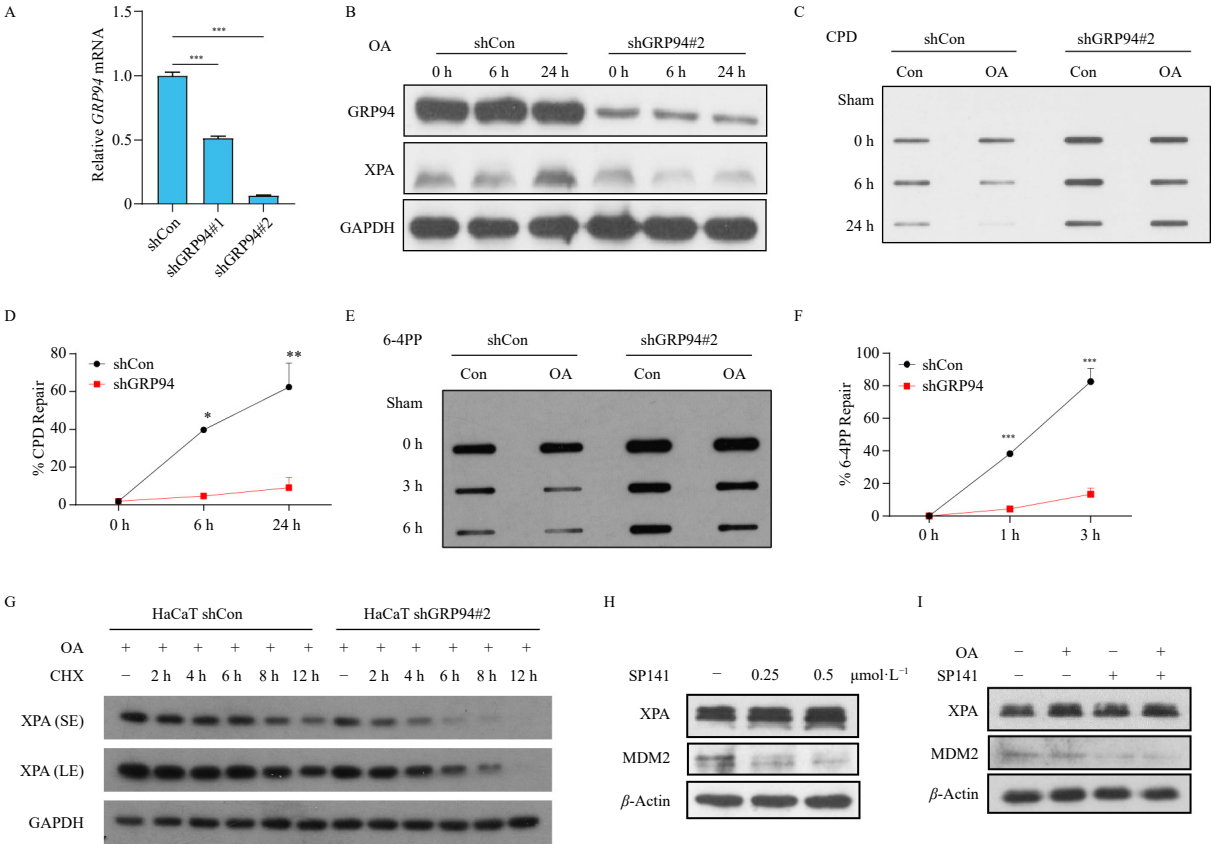

Fig. 7 Oroxylin A stabilizes XPA and inhibits its degradation *via* the proteasome pathway. (A) RT-qPCR assay of *GRP94* in HaCaT cells stably transfected with control shRNA or 2 independent shRNAs targeting GRP94 (GRP94 shRNA#1 and GRP94 shRNA#2). Differences are tested using one-way ANOVA. (B) Representative immunoblot analysis of GRP94, XPA, and GAPDH in HaCaT cells stably transfected with control shRNA or shGRP94. (C) Slot blot analysis of the levels of CPD in HaCaT shCon and shGRP94 cells at 0, 6, and 24 h post-UVB irradiation (5 mJ·cm^{-2}) and (D) Quantification of percentage (%) of CPD repair. (E) Slot blot analysis of the levels of 6-4PP in HaCaT shCon and shGRP94 cells at 0, 1, and 3 h post-UVB irradiation (5 mJ·cm^{-2}) and (F) quantification of percentage (%) of 6-4PP repair. (G) Western blot analysis of XPA in HaCaT shCon and shGRP94 cells treated with 50 μmol·L^{-1} oroxylin A and then with CHX (100 mg·mL^{-1}) for different times. (H) Impact of 0.25 or 0.5 μmol·L^{-1} MDM2 inhibitor SP141 on expression of MDM2 and XPA in HaCaT cells. (I) OA-induced addition of XPA was increased after treatment with 0.5 μmol·L^{-1} SP141. Data are presented as mean ± SEM (n = 3), $^{*}P < 0.05$, $^{**}P < 0.01$, $^{***}P < 0.001$ *vs* shCon group (n.s. not significant). Differences are tested using two-way ANOVA.

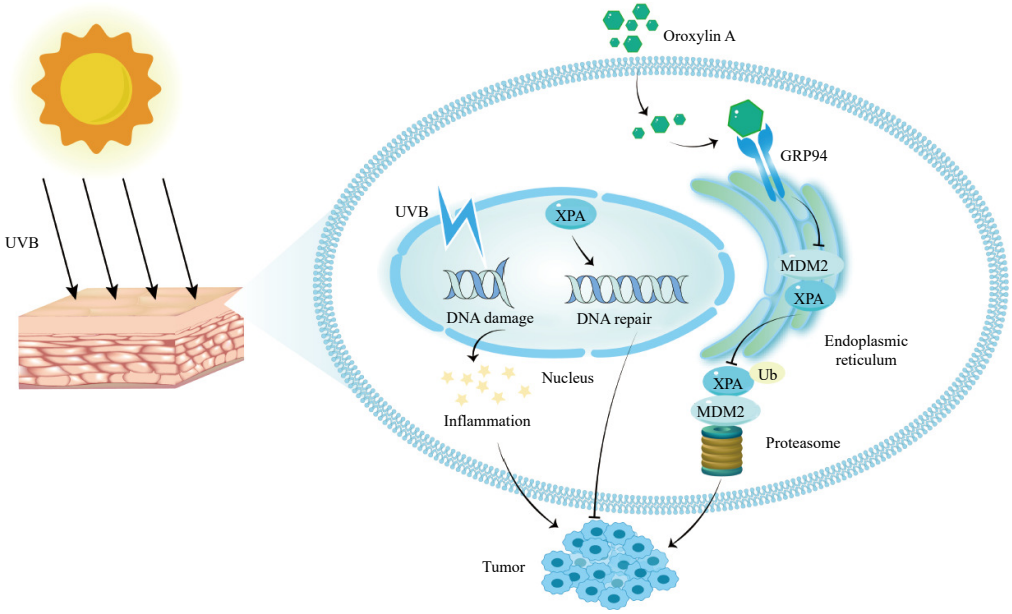

Fig. 8 Oroxylin A stabilizes XPA *via* binding GRP94 and inhibits XPA degradation through the MDM2-mediated proteasome pathway.

shock protein 90 (HSP90) family [49, 50]. However, our findings suggest that OA does not affect GRP94 transcription or expression. GRP94 possesses an atypical nucleotide binding pocket containing aromatic amino acids such as Phe199, which likely facilitate π-stacking interactions [51, 52]. Current GRP94 inhibitor development strategies target Phe199, and several inhibitors have been developed based on anti-inflammatory effects [53, 54]. Our results demonstrate that OA can form hydrogen bonds with Phe199.

Consequently, we hypothesize that OA may influence the conformation of GRP94 by binding to its Phe199 site, a speculation that warrants further investigation.

In conclusion, this study demonstrates that OA has the potential to delay the onset of UVB-induced NMSC and mitigate UVB-induced acute skin damage (Fig. 8). The primary mechanism involves OA's role in facilitating NER by preserving XPA stability. This is achieved through the disruption of GRP94 interactions with MDM2, which subsequently inhibits MDM2-mediated XPA ubiquitination and degradation. Consequently, OA emerges as a promising chemoprotective agent against the development of NMSC. This research presents OA as a potential candidate for the prevention of NMSC, offering new possibilities in dermatological oncology prevention.

Funding

This work was supported by the National Natural Science Foundation of China (No. 81974425), the Natural Science Foundation of Jiangsu Province (Nos. BK20211578 and BK20210419), the China Postdoctoral Science Foundation Grant (No. 2021M693513), and the Postgraduate Research & Practice Innovation Program of Jiangsu Province (No. KYCX22-0794).

Availability of supporting information

Supporting information for this work can be obtained by contacting the corresponding authors *via* E-mail.

Declaration of competing interest

The authors declare no conflict of interest.

References

1 Kocarnik JM, Compton K, Dean FE, et al. Cancer incidence, mortality, years of life lost, years lived with disability, and disability-adjusted life years for 29 cancer groups from 2010 to 2019: a systematic analysis for the global burden of disease study 2019. *JAMA Oncol*. 2022;8(3):420-444. https://doi.org/10.1001/jamaoncol.2021.6987.
2 Zink A. Trends in the treatment and prevention of keratinocyte carcinoma (non-melanoma skin cancer). *Curr Opin Pharmacol*. 2019;46:19-23. https://doi.org/10.1016/j.coph.2018.12.002.
3 Didona D, Paolino G, Bottoni U, et al. Non melanoma skin cancer pathogenesis overview. *Biomedicines*. 2018;6(1):6. https://doi.org/10.3390/biomedicines6010006.
4 Smith H, Wernham A, Patel A. When to suspect a non-melanoma skin cancer. *BMJ*. 2020;368:m692. https://doi.org/10.1136/bmj.m692.
5 Winge MC, Kellman LN, Guo K, et al. Advances in cutaneous squamous cell carcinoma. *Nat Rev Cancer*. 2023;23(7):430-449. https://doi.org/10.1038/s41568-023-00583-5.
6 Bernard JJ, Gallo RL, Krutmann J. Photoimmunology: how ultraviolet radiation affects the immune system. *Nat Rev Immunol*. 2019;19(11):688-701. https://doi.org/10.1038/s41577-019-0185-9.
7 Estadt SN, Maz MP, Musai J, et al. Mechanisms of photosensitivity in autoimmunity. *J Invest Dermatol*. 2022;142(3):849-856. https://doi.org/10.1016/j.jid.2021.05.007.
8 Salminen A, Kaarniranta K, Kauppinen A. Photoaging: UV radiation-induced inflammation and immunosuppression accelerate the aging process in the skin. *Inflamm Res*. 2022;71(7):817-831. https://doi.org/10.1007/s00011-022-01598-8.
9 Nieto MN, Olthof AM, Svejstrup JQ. Transcription-coupled nucleotide excision repair and the transcriptional response to UV-induced DNA damage. *Annu Rev Biochem*. 2023;92:81-113. https://doi.org/10.1146/annurev-biochem-052621-091205.
10 Martens MC, Emmert S, Boeckmann L. Sunlight, vitamin D, and xeroderma pigmentosum. *Adv Exp Med Biol*, 2020;1268:319-331. https://doi.org/10.1007/978-3-030-46227-7_16.
11 Sugitani N, Sivley RM, Perry KE, et al. XPA: a key scaffold for human nucleotide excision repair. *DNA Repair*. 2016;44:123-135. https://doi.org/10.1016/j.dnarep.2016.05.018.
12 Kim J, Li CL, Chen X, et al. Lesion recognition by XPC, TFIIH and XPA in DNA excision repair. *Nature*. 2023;617(7959):170-175. https://doi.org/10.1038/s41586-023-05959-z.
13 Borszéková PL, Ward TA, Chovanec M. XPA: DNA repair protein of significant clinical importance. *Int J Mol Sci*. 2020;21(6):2182. https://doi.org/10.3390/ijms21062182.
14 Jiang H, Yang LY. Cell cycle checkpoint abrogator UCN-01 inhibits DNA repair: association with attenuation of the interaction of XPA and ERCC1 nucleotide excision repair proteins. *Cancer Res*. 1999;59(18):4529-4534.
15 Barret JM, Cadou M, Hill BT. Inhibition of nucleotide excision repair and sensitisation of cells to DNA cross-linking anticancer drugs by F11782, a novel fluorinated epipodophylloid. *Biochem Pharmacol*. 2002;63(2):251-258. https://doi.org/10.1016/S0006-2952(01)00835-8.
16 Aune GJ, Furuta T, Pommier Y. Ecteinascidin 743: a novel anticancer drug with a unique mechanism of action. *Anticancer Drugs*. 2002;13(6):545-555. https://doi.org/10.1097/00001813-200207000-00001.
17 Neher TM, Shuck SC, Liu JY, et al. Identification of novel small molecule inhibitors of the XPA protein using *in silico* based screening. *ACS Chem Biol*. 2010;5(10):953-965. https://doi.org/10.1021/cb1000444.
18 Yao JY, Xu S, Sun YN, et al. Novel CDK9 inhibitor oroxylin A promotes wild-type P53 stability and prevents hepatocellular carcinoma progression by disrupting both MDM2 and SIRT1 signaling. *Acta Pharmacol Sin*. 2022;43(4):1033-1045. https://doi.org/10.1038/s41401-021-00708-2.
19 Huo TX, Wang XP, Yu Z, et al. Oroxylin A inhibits the migration of hepatocellular carcinoma cells by inducing NAG-1 expression. *Acta Pharmacol Sin*. 2022;43(3):724-734. https://doi.org/10.1038/s41401-021-00695-4.
20 Cao Y, Cao W, Qiu Y, et al. Oroxylin A suppresses ACTN1 expression to inactivate cancer-associated fibroblasts and restrain breast cancer metastasis. *Pharmacol Res*. 2020;159:104981. https://doi.org/10.1016/j.phrs.2020.104981.
21 Wei M, Ma R, Huang S, et al. Oroxylin A increases the sensitivity of temozolomide on glioma cells by hypoxia-inducible factor 1α/hedgehog pathway under hypoxia. *J Cell Physiol*. 2019;234(10):17392-17404. https://doi.org/10.1002/jcp.28361.
22 Qiang L, Sample A, Shea CR, et al. Autophagy gene *ATG7* regulates ultraviolet radiation-induced inflammation and skin tumorigenesis. *Autophagy*. 2017;13(12):2086-2103. https://doi.org/10.1080/15548627.2017.1380757.
23 Li B, Birt DF. *In vivo* and *in vitro* percutaneous absorption of cancer preventive flavonoid apigenin in different vehicles in mouse skin. *Pharm Res*. 1996;13:1710-1715. https://doi.org/10.1023/A:1016453009818.
24 Li B, Pinch H, Birt DR. Influence of vehicle, distant topical delivery, and biotransformation on the chemopreventive activity of apigenin, a plant flavonoid, in mouse skin. *Pharm Res*. 1996;13:1530-1534. https://doi.org/10.1023/A:1016083613916.
25 Qiang L, Zhao B, Shah P, et al. Autophagy positively regulates DNA damage recognition by nucleotide excision repair. *Autophagy*. 2016;12(2):357-368. https://doi.org/10.1080/15548627.2015.1110667.
26 Bowden GT. Prevention of non-melanoma skin cancer by targeting ultraviolet-B-light signalling. *Nat Re Cancer*. 2004;4(1):23-35. https://doi.org/10.1038/nrc1253.
27 Montes de OMK, Pearlman RL, Mcclees SF, et al. Phytochemicals for the prevention of photocarcinogenesis. *Photochem Photobiol*. 2017;93(4):956-974. https://doi.org/10.1111/php.12711.
28 Liu Y, Wang X, Li W, et al. Oroxylin A reverses hypoxia-induced cisplatin resistance through inhibiting HIF-1α mediated XPC transcription. *Oncogene*. 2020;39(45):6893-6905. https://doi.org/10.1038/s41388-020-01474-x.
29 de Oliveira AN, Pereira GM, di Domenico M, et al. Inflammation response, oxidative stress and DNA damage caused by urban air pollution exposure increase in the lack of DNA repair XPC protein. *Environ Int*. 2020;145:106150. https://doi.org/10.1016/j.envint.2020.106150.
30 Kunisada M, Hosaka C, Takemori C, et al. CXCL1 inhibition regulates UVB-induced skin inflammation and tumorigenesis in Xpa-deficient mice. *J Invest Dermatol*. 2017;137(9):1975-1983. https://doi.org/10.1016/j.jid.2017.04.034.
31 Kunisada M, Yamano N, Hosaka C, et al. Inflammation due to voriconazole-induced photosensitivity enhanced skin phototumorigenesis in Xpa-knockout mice. *Photochem Photobiol*. 2018;94(5):1077-1081. https://doi.org/10.1111/php.12972.
32 Huck JD, Que NL, Hong F, et al. Structural and functional analysis of GRP94 in the closed state reveals an essential role for the pre-N domain and a potential client-binding site. *Cell Rep*. 2017;20(12):2800-2809. https://doi.org/10.1016/j.celrep.2017.08.079.
33 Wu B, Chu X, Feng C, et al. Heat shock protein gp96 decreases p53 stability by regulating Mdm2 E3 ligase activity in liver cancer. *Cancer Lett*. 2015;359(2):325-334. https://doi.org/10.1016/j.canlet.2015.01.034.
34 Apalla Z, Lallas A, Sotiriou E, et al. Epidemiological trends in skin cancer. *Dermatol Pract Conce*. 2017;7(2):1-6. https://doi.org/10.5826/dpc.0702a01.
35 Olsen CM, Pandeya N, Ragaini BS, et al. International patterns and trends in the incidence of melanoma and cutaneous squamous cell carcinoma, 1989–2020. *Brit J Dermatol*. 2024;190(4):492-500. https://doi.org/10.1093/bjd/ljad425.
36 Katiyar SK, Pal HC, Prasad R. Dietary proanthocyanidins prevent ultraviolet radiation-induced non-melanoma skin cancer through enhanced repair of damaged DNA-dependent activation of immune sensitivity. *Semin Cancer Biol*. 2017;46:138-145. https://doi.org/10.1016/j.semcancer.2017.04.003.
37 Huang H, Cai H, Zhang L, et al. Oroxylin A inhibits carcinogen-induced skin tumorigenesis through inhibition of inflammation by regulating SHCBP1 in mice. *Int Immuno*. 2020;80:106123. https://doi.org/10.1016/j.intimp.2019.106123.
38 Greten FR, Grivennikov SI. Inflammation and cancer: triggers, mechanisms, and consequences. *Immunity*. 2019;51(1):27-41. https://doi.org/10.1016/j.immuni.2019.06.025.
39 Locati M, Curtale G, Mantovani A. Diversity, mechanisms, and significance of macrophage plasticity. *Annu Rev Pathol-Mech*. 2020;15:123-147. https://doi.org/10.1146/annurev-pathmechdis-012418-012718.
40 Klapp V, Álvarez-abril B, Leuzzi G, et al. The DNA damage response and inflammation in cancer. *Cancer Discov*. 2023;13(7):1521-1545. https://doi.org/10.1158/2159-8290.CD-22-1220.
41 Piotrowski I, Kulcenty K, Suchorska W. Interplay between inflammation and

cancer. *Rep Pract Oncol Radi*. 2020;25(3):422-427. https://doi.org/10.1016/j.rpor.2020.04.004.
42 Chen DH, Zheng G, Zhong XY, et al. Oroxylin A attenuates osteoarthritis progression by dual inhibition of cell inflammation and hypertrophy. *Food Funct*. 2021;12(1):328-329. https://doi.org/10.1039/D0FO02159H.
43 Yang J, Li J, Wang J, et al. Oroxylin A relieves intrauterine adhesion in mice through inhibiting macrophage pyroptosis *via* SIRT3-SOD2-ROS pathway. *Int Immunopharmacol*. 2023;118:110023. https://doi.org/10.1016/j.intimp.2023.110023.
44 Sahan AZ, Hazra TK, Das S. The pivotal role of DNA repair in infection mediated-inflammation and cancer. *Front Microbiol*. 2018;9:663. https://doi.org/10.3389/fmicb.2018.00663.
45 Taffoni C, Marines J, Chamma H, et al. DNA damage repair kinase DNA-PK and cGAS synergize to induce cancer-related inflammation in glioblastoma. *EMBO J*. 2023;42(7):e111961. https://doi.org/10.15252/embj.2022111961.
46 Chatterjee N, Walker GC. Mechanisms of DNA damage, repair, and mutagenesis. *Environ Mol Mutagen*. 2017;58(5):235-263. https://doi.org/10.1002/em.22087.
47 Horio T, Miyauchi-hashimoto H, Kuwamoto K, et al. Photobiological information obtained from *XPA* gene-deficient mice. *Photochem Photobiol*. 2007;83(1):218-224. https://doi.org/10.1562/2006-03-02-IR-829.
48 Duan X, Iwanowycz S, Ngoi S, et al. Molecular chaperone GRP94/GP96 in cancers: oncogenesis and therapeutic target. *Front Oncol*. 2021;11:629846. https://doi.org/10.3389/fonc.2021.629846.
49 Senft D, Ze'ev AR. UPR, autophagy, and mitochondria crosstalk underlies the ER stress response. *Trends Biochem Sci*. 2015;40(3):141-148. https://doi.org/10.1016/j.tibs.2015.01.002.
50 Lee AS. Glucose-regulated proteins in cancer: molecular mechanisms and therapeutic potential. *Nat Rev Cancer*. 2014;14(4):263-276. https://doi.org/10.1038/nrc3701.
51 Birbo B, Madu EE, Madu CO, et al. Role of HSP90 in cancer. *Int J Mol Sci*. 2021;22(19):10317. https://doi.org/10.3390/ijms221910317.
52 Duerfeldt AS, Peterson LB, Maynard JC, et al. Development of a Grp94 inhibitor. *J Am Chem Soc*. 2012;134(23):9796-9804. https://doi.org/10.1021/ja303477g.
53 Xu S, Guo A, Chen NN, et al. Design and synthesis of Grp94 selective inhibitors based on Phe199 induced fit mechanism and their anti-inflammatory effects. *Eur J Med Chem*. 2021;223:113604. https://doi.org/10.1016/j.ejmech.2021.113604.
54 Jiang F, Guo AP, Xu JC, et al. Discovery of a potent Grp94 selective inhibitor with anti-inflammatory efficacy in a mouse model of ulcerative colitis. *J Med Chem*. 2018;61(21):9513-9533. https://doi.org/10.1021/acs.jmedchem.8b00800.